Gold Bulletin (2025) 58:10
https://doi.org/10.1007/s13404-025-00363-z

RESEARCH

Nanosecond-pulsed laser ablation synthesis of gold nanoparticles in DDDW, NaOH, and DMEM liquid media: unveiling of microstructural morphological, chemical, optical, and structural characterizations and cytotoxic evaluation of enhanced anticancer efficacy

Entidhar Jasim Khamees[1] · Elaf Yousif Rashid[1] · Zainab Hayder Jabber Al-Kufaishi[1] · Kahtan A. Mohammed[2,3] · Rajaa Ali Mohesiseen Al-Taee[1] · Shubham Sharma[4,5,11] · Teku Kalyani[6] · Manish Sharma[7] · Ankur Kulshreshta[8] · Abhinav Kumar[9] · Krishnaraj Ramaswamy[10]

Received: 14 October 2024 / Accepted: 23 April 2025 / Published online: 5 May 2025

Abstract

Synthesis of gold nanoparticles (AuNPs) in the presence of three different liquid mediums was carried out using ns-pulsed laser ablation in liquid: DDDW, NaOH, and DMEM. X-ray diffraction (XRD), atomic force microscopy (AFM), transmission electron microscopic investigations (TEM), Fourier transform infrared (FTIR), and UV–visible spectroscopy were some of the techniques that were utilized in order to describe the structural, chemical, morphological, topological, and optical features of as-produced nanomaterials. The characterization studies provided evidence that the successful synthesis route was appropriate. It has been demonstrated via the utilization of cytotoxicity tests that gold nanoparticles have the capacity to not only eradicate cancer cells but also stop their reproduction. This ability was demonstrated by gold nanoparticles. The Au nanoparticles showed an extraordinarily deadly efficacy against cancer cells as compared to cancer cells that had not been treated with the chemical. This was accomplished by preventing the growth and reproduction of cancer cells.

Keywords Nanotechnology · AuNPs · Laser ablation · Anticancer agent

✉ Kahtan A. Mohammed
kahtan444@gmail.com

✉ Shubham Sharma
shubham543sharma@gmail.com;
shubhamsharmacsirclri@gmail.com

[1] Department of Physiology and Medical Physics, College of Medicine, University of Babylon, City of Hilla, Babylon, Iraq

[2] Department of Medical Physics, Faculty of Medical Sciences, Jabir Ibn Hayyan Medical University, Najaf, Iraq

[3] Department of Medical Physics, Hilla University College, Babylon, Iraq

[4] Department of Technical Sciences, Western Caspian University, Baku, Azerbaijan

[5] Centre for Research Impact and Outcome, Chitkara University Institute of Engineering and Technology, Chitkara University, Rajpura 140401, Punjab, India

[6] Department of Mechanical Engineering, Raghu Engineering College, Dakamarri 531162, Andhra Pradesh, India

[7] Department of Mechanical Engineering, Chandigarh College of Engineering, Chandigarh Group of Colleges, Jhanjeri, Mohali 140307, Punjab, India

[8] Department of Mechanical Engineering, NIMS University, Jaipur, Rajasthan, India

[9] Department of Nuclear and Renewable Energy, Ural Federal University Named After the First President of Russia, Boris Yeltsin, 19 Mira Street, 620002 Yekaterinburg, Russia

[10] Department of Mechanical Engineering, Dambi Dollo University, Dembi Dolo, Ethiopia

[11] Jadara University Research Center, Jadara University, Irbid, Jordan

Introduction

Nanoparticles (NPs), in the form of noble metals, are well known to be important materials in a wide variety of basic and applied research domains. These fields include catalysis, optics, fuel cells, and medicine [1–4]. Because of the potential applications that noble metal nanoparticles could have in a variety of sectors, including chemistry, materials science, physics, medicine, biology, and engineering, they have garnered a substantial amount of attention in recent years. AuNPs are particularly interesting due to the singular characteristics that they possess [5–7]. Many types of noble metals can be prepared, studied, and applied in the field of medicine and biology like copper, silver, and gold [8, 9].

Because of its one-of-a-kind properties, such as nontoxicity, easy availability with controlled particle size and shape, increased particle reactivity, surface modification capacity, and high optical characteristics, gold nanoparticles, also known as AuNPs, are the subject of intensive research in a variety of applications, ranging from the material sciences to the medical sciences. Because of a phenomenon known as localized surface plasmon resonance (LSPR), gold nanoparticles exhibit a color that may be described as either red or purple at a wavelength that is close to 530 nm. It is possible to alter the properties of AuNPs through the manipulation of their size, shape, and surface modification through the use of synthetic techniques [10–16]. Surface plasmons result in a variety of novel functional characteristics, such as powerful resonant absorption/scattering, spectacular field augmentation, optical navigation, and ultrasensitive biosensors. Their strong optical absorption has been used for light-induced hyperthermy of solid cancers; their cross section is typically 105 times higher than that of absorbing dyes. In addition to providing contrast for photoacoustic or light scattering-based cancer imaging, Au-NPs can also be used to generate movable surface-enhanced Raman scattering-based tags for cancer targeting and diagnostics [17, 18].

Synthesizing gold nanoparticles can be done chemically or physically. Stable gold nanoparticles with plasmon absorption peaks in the visible to near infrared wavelength region can be made using chemical techniques using reducing agents and stabilizing surfactants. However, the process results in potentially dangerous byproducts. Gold nanoparticles have been created using a physical approach called pulse laser ablation [19, 20].

When a laser beam hits a target, it removes the material off the surface of the target and, in doing so, promotes the production of nanoparticles in a liquid surrounded by vapor. The room-temperature solid surface layer of the target undergoes melting at high enough laser fluence. Overheating transforms the normal liquid medium around the target into a gaseous state. The high-pressure vapor reacts with the molten layer on the target surface, creating nanoparticles that are then dispersed into the surrounding liquid. A wide range of nanoparticles can be synthesized using laser ablation of solids in liquid. Due to its ease of use and potential for producing chemically pure nanoparticles, this method is currently receiving a great deal of attention [21, 22].

The present study is going to explore the implications of the medium employed for the synthesis of gold nanoparticles on the characteristics of the resulting nanoparticles.

For these reasons, we used laser ablation technology, a viable and affordable approach that has not been extensively researched, to create gold nanoparticles. Our goal is to use various laser fluids to alter the size and surface shape of gold nanoparticles and assess the results. By lowering the toxicity of nanomaterials and increasing cell penetration, the ultimate objective is to increase the ability of gold nanoparticles to enter cancer cells. This technique is crucial for figuring out the size, particularly in applications involving photothermal treatment (PTT) [23].

Experimentation: materials and methods

Experimental details production of AuNPs

Metal nanoparticles in liquid were created using a multimedia laser ablation technique. A lens, a high-power pulsed laser, a liquid vessel, a motor, and a linear positioner make up the majority of the laser ablation system. Dulbecco's Modified Medium (DMEM), which contained distilled water, sodium hydroxide (NaOH), and double deionized water (DDDW), was submerged in a metal target, such as gold (99.99%). The metal plate was ablated using a pulsed Nd:YAG laser at a wavelength of 532 or 1064 nm. A Q-switched Nd:YAG laser, a solution vessel, a metal plate, a lens with a focal length of 30 cm, a linear transition stage, and a motor were all included in the system. The laser ablation time and pulse duration may be adjusted from 5 to 60 min and 10 to 60 Hz, respectively. The laser beam travel length through the liquid was set to the minimum length feasible in order to stop the energy from the beam from being absorbed into the liquid solution. Therefore, the distance among the target as well as the entrance windows is one of the most critical factors in achieving the optimal laser beam energy on the target surface. This assures that the metal nanoparticles are distributed homogeneously all throughout the liquid solution. For three solutions, in order to determine the pulse repetition rate and duration that correspond to these energies, the values of 300 pulses, 10 ns, and 6 Hz were chosen. Figure 1a and b depicts the laser ablation techniques

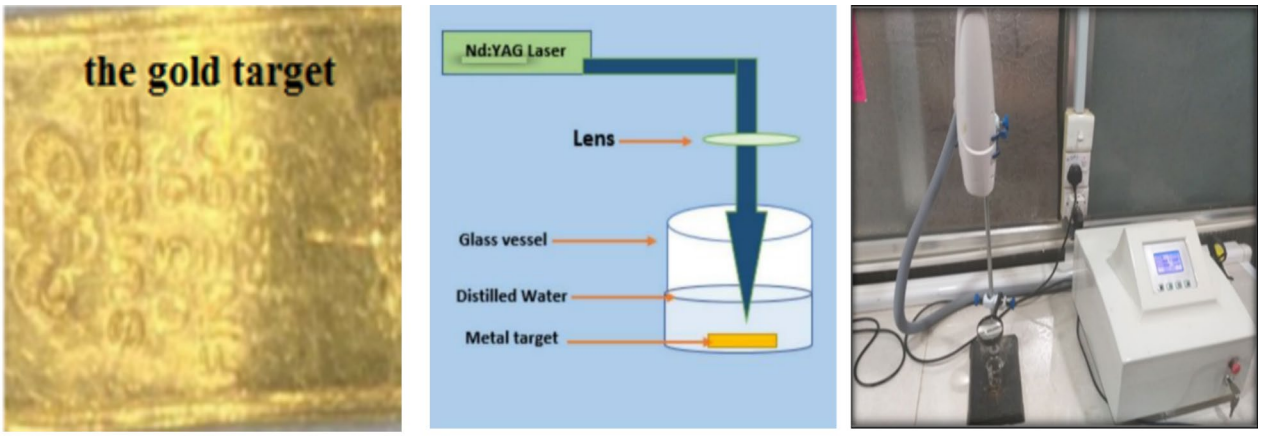

Fig. 1 **a**, **b** Scheme of the laser device, Nd-YAG laser and the gold target

in a liquid medium image. X-ray diffraction, atomic force microscopy (AFM), and transmission electron microscopy (TEM) are only a few of the experimental methods used to determine the characteristics and morphology of man-made materials. UV–Vis spectrophotometer was used to measure the peaks of SPR, and the results showed a linear relationship with size.

Anticancer activity testing

Cell lines and culture

In the investigation, Hepa 1–6 mouse cell lines and culture were sourced from the National Cell Bank of Iran. The cells were grown in RPMI-1640 with 10% FBS supplemented with antibiotics and maintained at 37 °C under humidified air. The MTT cell viability assay was used to quantify cell growth and viability. The cells were digested, harvested, and seeded into 96-well plates. When forming a monolayer, they were treated with a DMSO solution for 24 h at 37 °C in 5% CO2. After 24 h, the supernatant was removed, and 200 µl/well of MTT solution was added. The cells were incubated on a shaker at 37 °C until crystals were completely dissolved. The concentration of compounds that resulted in 50% of cell death (IC50) was determined from respective dose–response curves.

Cytotoxicity assay

In order to determine whether or not AuNPs are cytotoxic to cell lines, a test using MTT (3-(4,5-dimethylthiazol-2-yl)−2,5-diphenyltetrazolium bromide) was carried out. The process was carried out correctly in accordance with [2, 24–26].

Statistical analysis

The data that were presented in the findings section were all presented as the mean along with the standard deviation. Sigma plot v12 software was used to perform an analysis of variance (ANOVA) on the data using a one-way analysis of the data.

Results and discussions

XRD structural analysis

The X-ray diffraction morphologies of AuNPs liquid samples with varying colloidal solutions are illustrated in Figure 2. The diffraction peaks of XRD measurement are observed around 37.8248°, 43.6291°, 64.2015°, and 77.2181°, 37.4471°, 43.6634°, 64.1671°, and 77.0807°, and 37.9279°, 43.6291°, 63.9267°, and 77.0464° for Au nanoparticle sizes 4, 8, and 13 nm, respectively, as exhibited in Table 1. These peaks can be assigned to diffraction from (111), (200), (220), and (311) planes, respectively [27]. The Scherrer formula's purpose was to determine the crystallite size [27]. X-ray diffraction (XRD) characterization is carried out so that further confirmation of the structural properties of the generated samples can be obtained. The XRD results of all of the samples that were prepared are displayed in Fig. 2. The structure of the face-centered cubic Au phase can be seen in the pattern displayed by AuNPs (JCPDS no. 96–901–2954) [27].

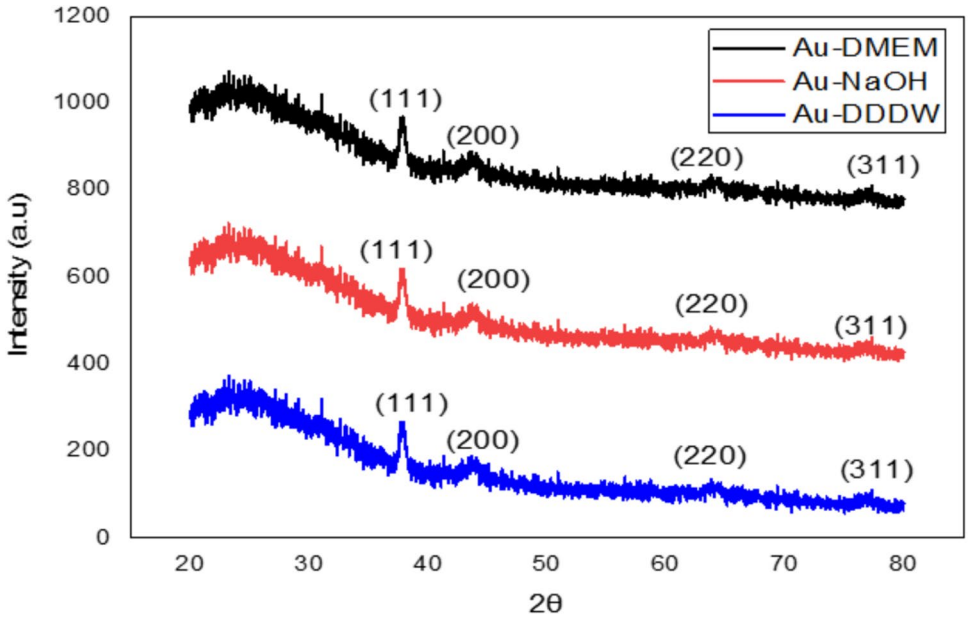

Fig. 2 XRD patterns of Au Nanoparticles prepared with different medium

Table 1 XRD pattern outcomes for liquid samples with different the colloidal solutions

Samples	2θ (°)	FWHM (°)	dhkl Exp.(A)	c.s	dhkl Std.(A)	Phase	hkl	JCPDS card number
AuNPs-NaOH	37.8248	0.4465	2.3766	18.8	2.3498	Cub. Au	111	96–901–2954
	43.6291	0.893	0.893	9.6	2.035	Cub. Au	200	96–901–2955
	64.2015	0.6525	1.4495	14.4	14.4	Cub. Au	220	96–901–2956
	77.2181	0.8928	1.2344	11.4	1.2271	Cub. Au	311	96–901–2957
AuNPs-DM EM	37.4471	0.7556	2.3997	11.1	2.3498	Cub. Au	111	96–901–2958
	43.6634	0.5839	2.0714	14.7	2.035	Cub. Au	200	96–901–2959
	64.1671	0.7899	1.4502	11.9	1.4389	Cub. Au	220	96–901–2960
	77.0807	0.5151	1.2363	19.7	19.7	Cub. Au	311	96–901–2961
AuNPs-DDW	37.9279	0.9959	2.3703	8.4	2.3498	Cub. Au	111	96–901–2962
	43.6291	0.4807	2.0729	17.8	2.035	Cub. Au	200	96–901–2963
	63.9267	1.0646	1.4551	8.8	1.4389	Cub. Au	220	96–901–2964
	77.0464	0.5837	1.2368	17.4	1.2271	Cub. Au	311	96–901–2965

The physicochemical interactions between prepared nanoparticles and the surrounding medium have been studied using FTIR spectroscopy. Figure 3 presents the Fourier transform infrared (FTIR) spectra of aqueous Au nanoparticles in the region of 4000 to 400 cm^{-1}. The investigation of the gold nanoparticles (AuNPs) was limited to FTIR in order to characterize the organic compounds that were engaged in the process of stabilizing the nanoparticle solution. For samples containing different colloidal solutions (Au-NaOH, Au-DMEM, and Au-DDW, respectively), the highest absorption bands were seen at 3428, 3430, and 3439 cm^{-1}. These bands were observed after the samples were extracted. The band located at 3500–3400 cm^{-1} is indicative of the stretching of the O–H bond. At 2500–2000) cm^{-1}, the band represents the stretching of C ≡ C and C ≡ N bonds. The frequency band of C-O stretching is displayed by the peak at 1700 – 1500 cm^{-1}. The C-H bands at 1000–500 cm^{-1} correspond to the carbonyl and hydroxyl functional groups in alcohols and phenol derivatives and are related to these groups [27]. According to the similarity, the compounds are identical in all AuNP media, regardless of the size of the particles. Presumably, the extract constituent's adsorption of AuNPs on [28] is responsible for the relatively small shifts in peaking positioning.

Atomic force microscope (AFM)

Examination of the outer surface of the gold nanoparticles was carried out by means of the atomic force microscope (AFM) technique. An essential collection of gold nanoparticles with a semi-spherical morphology is depicted in the two-dimensional photographs, which can be found

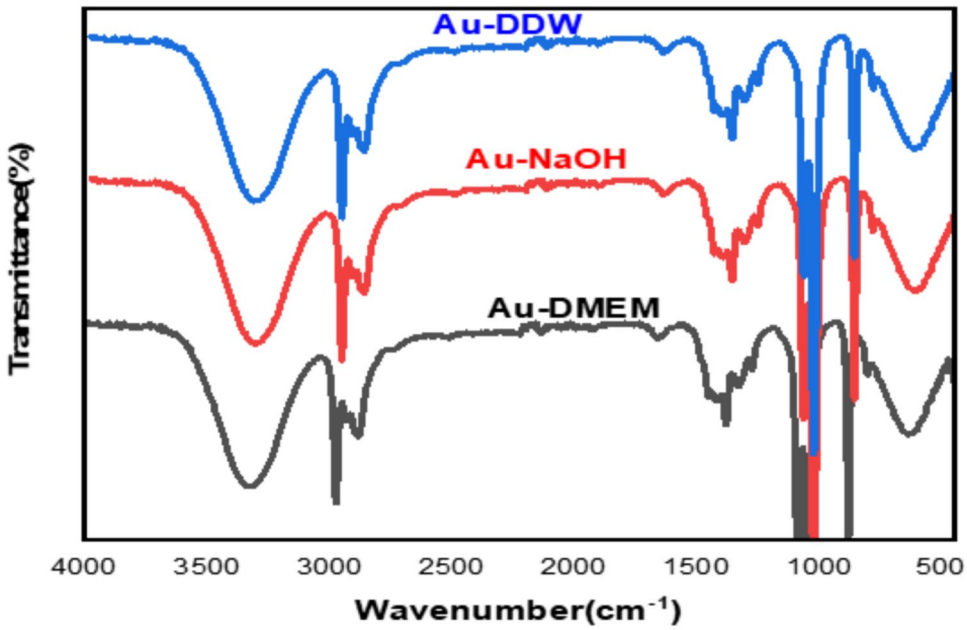

Fig. 3 FTIR spectra of Au NPs at different medium

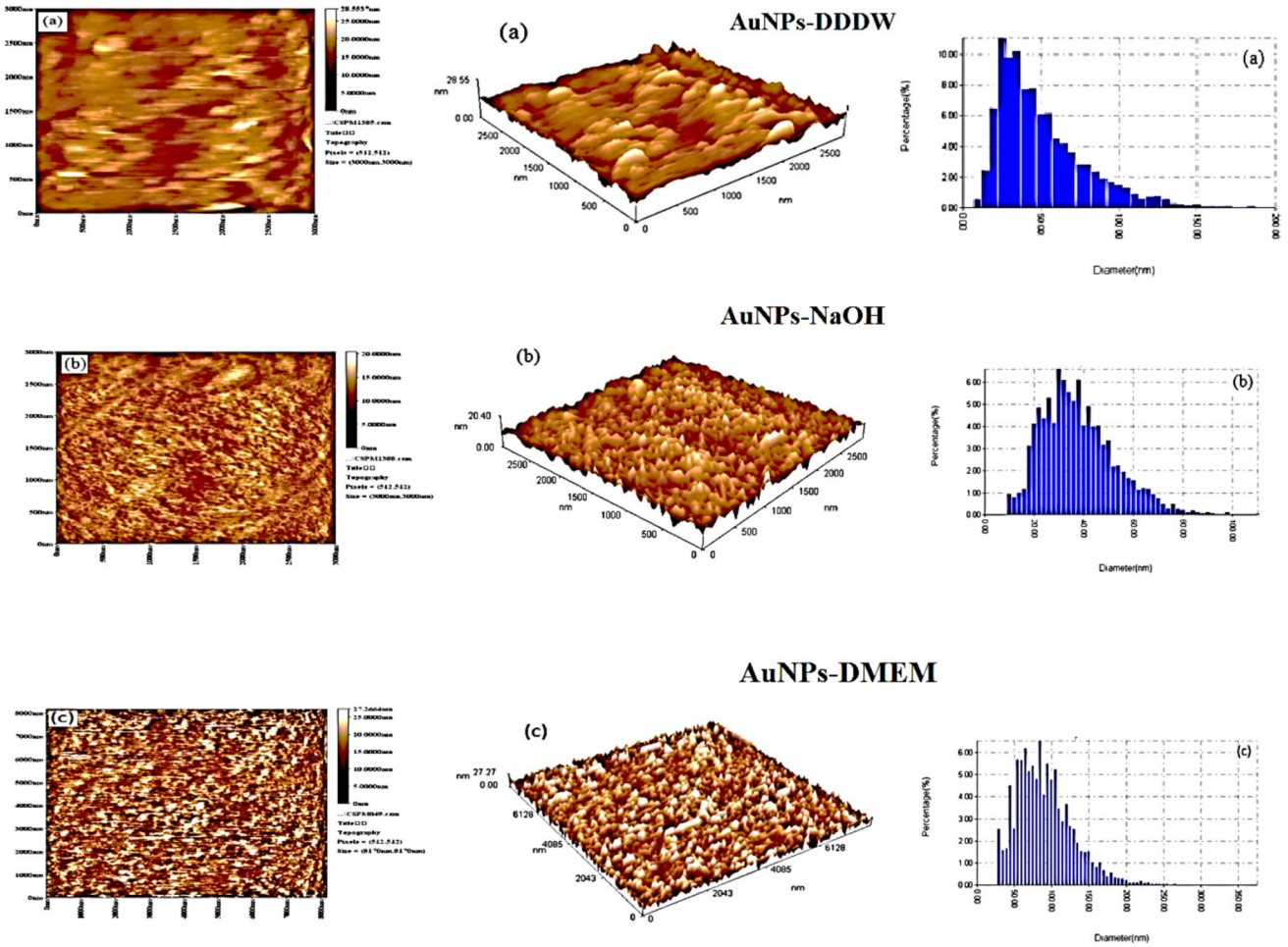

Fig. 4 **a** AFM and **b** three-dimensional images of a section of the nanoscale gold nanoparticles, **c** granularity commutation distribution chart for AuNPs samples at different prepared with DDDW, NaOH, and Dulbecco's Modified Medium (DMEM) of Au nanoparticles

in Fig. 4a–c. In order to obtain photos of gold nanoparticles, the following images were obtained: Au-DDDW, Au-NaOH, and Au-DMEM. The three-dimensional photographs of a segment of the nanoscale gold nanoparticles are displayed in Fig. 4d–f. It was found that the nanoscale gold nanoparticles had a high limit of 28.55, 20.40, and 27.27 nm for AuNPs at Au-DDDW, Au-NaOH, and Au-DMEM nm, respectively. These parameters were determined by the researchers. For the purpose of illustrating the granularity commutated, the distribution plot for gold nanoparticles (AuNPs) at various particle sizes was depicted in Fig. 4g–h. Furthermore, the AFM image particulate size dispersion revealed that the average diameter of the particles for AuNPs was around 48.6 nm, 63.8 nm, and 88.8 nm at Au-DDDW, Au-NaOH, and Au-DMEM nm, respectively. This was in contrast to the findings of the previous study. The average size of the grains of AuNPs at Au-DDDW, Au-NaOH, and Au-DMEM nm was 2484.9, 1241.8, and 7335.8 nm^2, respectively, as measured by AFM images. This information is presented in Table 2, which includes the results of the analysis.

Microstructural morphological analysis

The transmission electron microscope was used to evaluate morphology as well as particle dispersion. On top of the grid, a single drop of the colloidal suspension that included the Au NPs was deposited. Following that, the drop was allowed to dry at room temperature. Figure 5 presents TEM pictures of gold nanoparticles that were generated using a variety of different mediums. It is evident that the particles are nanosized and approximately spherical across all of the mediums employed. The smallest particle diameter is observed in the DMEM medium, with an average diameter of 5 nm. The largest particle diameter is achieved by using NaOH as a medium, with an average diameter of 25 nm.

UV–Vis spectroscopy of AuNPs

The formation of AuNPs was confirmed with UV–vis spectroscopy. The spectrum shows a very large peak at about 500–550 nm corresponding to the resonance of AuNPs plasmon. Figure 6, which reflects the peak of surface plasmon resonance of gold nanoparticles, displays the absorption spectra of aqueous AuNPs for different medium. Absorption spectra measurements were performed at room temperature for visible wavelengths ranging from 400 to 900 nm. It can be seen from Fig. 6 that l max is approximately 515, 524, and 521 nm for Au-DMEM, Au-NaOH, and Au-DDDW, respectively. Au nanoparticles have the good absorption in Vis region 500–600 nm BV [29].

Table 2 Surface parameters from AFM results

AuNPs	Min. diameter(nm)	Max. diameter (nm)	Average diameter (nm)
Au-DDDW	2	100	25.62
Au-NaOH	3.5	100	15.21
Au-DMEM	2.5	100	5.15

Biological implications of gold nanoparticles

The biological effects of gold nanoparticles were tested on cancer Hepa cell line grown in 96-hole plates, incubated with colloidal solutions for 24 h at 37 °C.

The samples were classified into four groups:

i. A group without treatment (control group)
ii. Treatment group for gold nanoparticles prepared in double distilled water (DDDW)
iii. The treatment group of gold nanoparticles prepared in NaOH
iv. Treatment group for gold nanoparticles prepared in DMEM culture medium

Cell killing percentages were calculated using the MTT test using a microtiter plate reader, and statistical calculations for each effect in isolation, and then according to the cumulative effect of all effects.

Connecting AuNPs with biological fluids is a crucial step in the therapeutic process to facilitate the endocytosis of AuNPs by cancer cells. This phase was finalized during the preparation phases of the nanoparticle production solutions via chemical or biological processes. In this study, the binding procedure was achieved by utilizing DMEM as the synthesis medium for the generated AuNPs via PLAL. AuNPs resulting from this process were larger than those prepared with NaOH and DDDW. The adsorption of protein compounds within DMEM by AuNPs resulted in localized shifting of absorption maxima.

The cytotoxic effect of AuNPs on Hepa cell line (cancer cells) is shown in Fig. 7. AuNPs-DDDW showed medium cytotoxicity but AuNPs-MDEM nanoparticles were more toxic than AuNPs-NaOH in concentration 12.5 µg/ml.

Figures 8 and 9 show the effects of AuNPs on the viability of Hepa cell line incubated for 24 h in the presence of different concentrations of AuNPs prepared using laser ablation technique. Synthetic AuNPs has possessed an anticancer properties. In comparison to the standard drug used for the study, the test compounds AuNPs demonstrated significant cytotoxic potential properties against Hepa 1–6 mouse cell lines, as confirmed by the statistical data of the cell cytotoxicity study by ELISA reader. The IC50

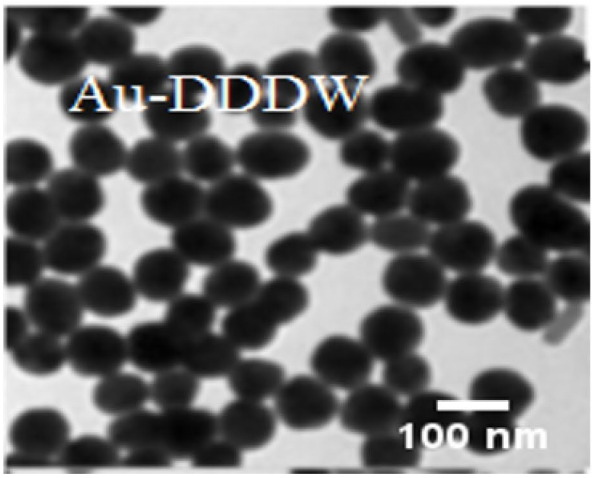

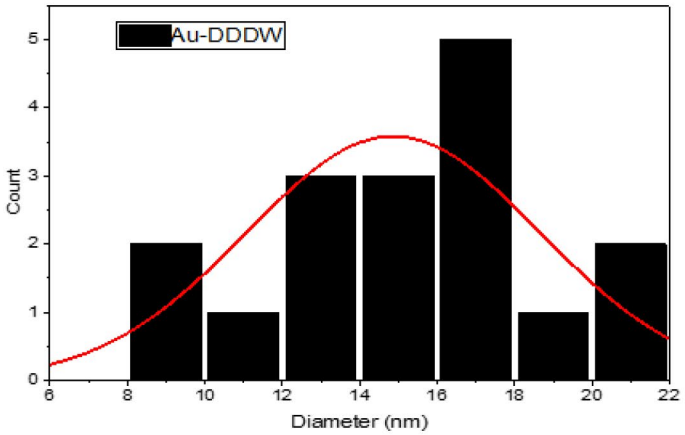

(a).

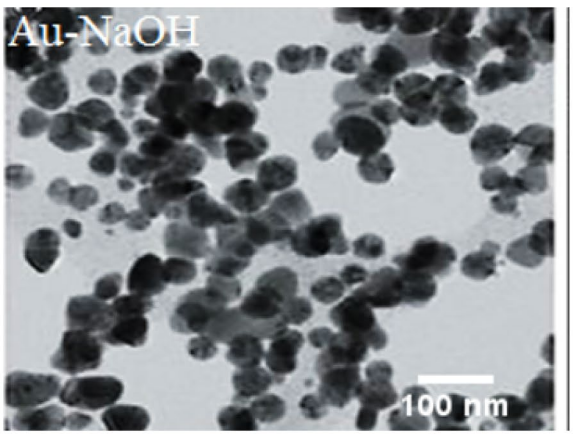

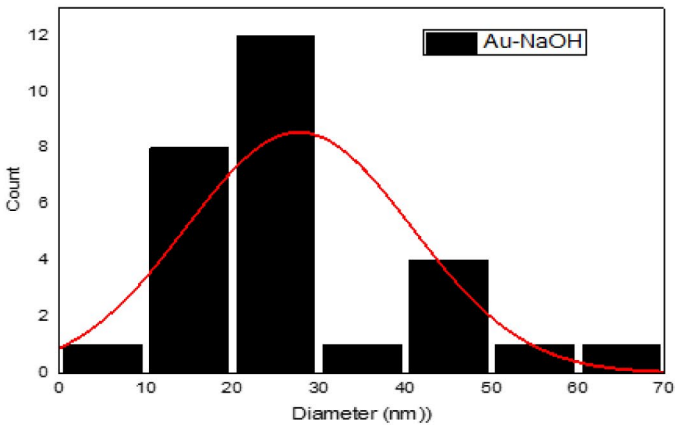

(b).

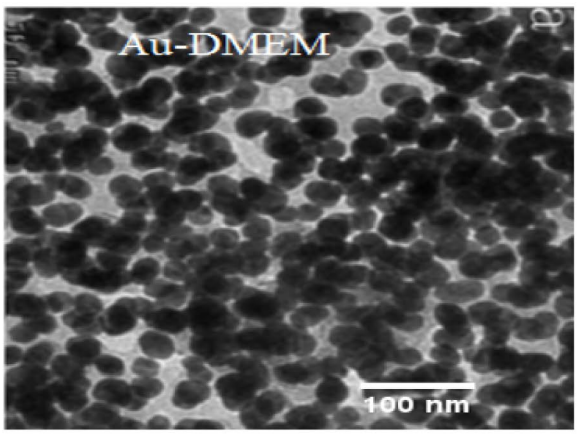

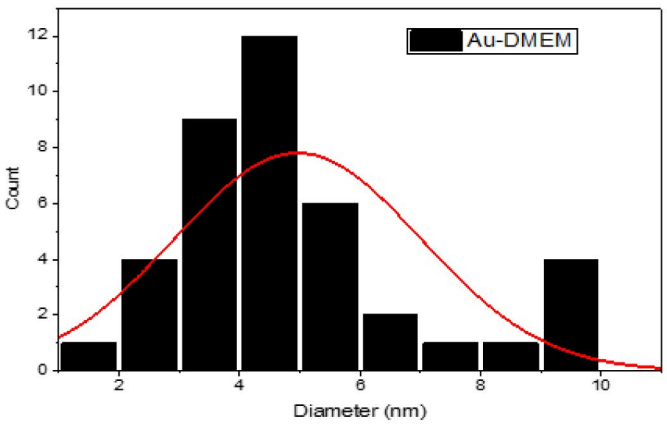

(c).

Fig. 5 TEM images of AuNPs: **a** Au-DDDW, **b** Au-NaOH, and **c** Au-DMEM of Au nanoparticles) at different mediums

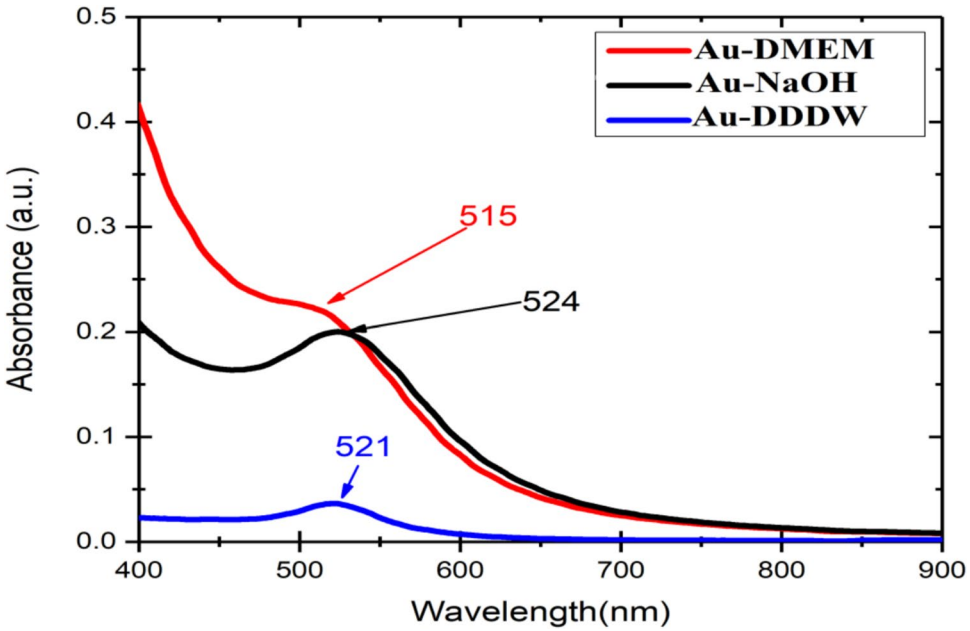

Fig. 6 UV–visible spectra of the Au NPs synthesized by laser ablation in different medium

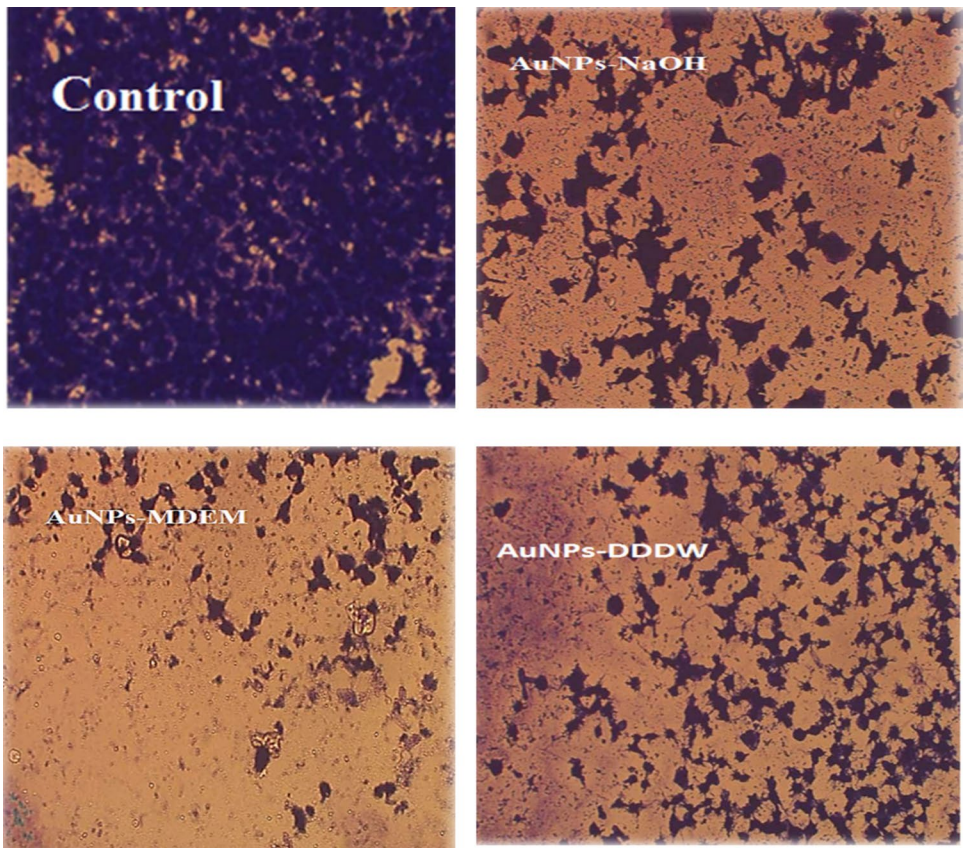

Fig. 7 Inverted microscope images of Hepa cell line before and after adding Au nanoparticles

concentrations were 53.95 µg/ml at the treatment group for gold nanoparticles prepared in double distilled water (DDDW) and 74.38 µg/ml and 35.48 µg/ml at the treatment group for gold nanoparticles prepared in NaOH and culture medium DMEM, respectively.

In the therapeutic chain, the process of attaching AuNPs to biological fluids is crucial for achieving AuNP endocytosis by cancer cells. In this work, the binding procedure was carried out by turning DMEM into a synthesis medium for the AuNPs that were synthesized by PLAL.

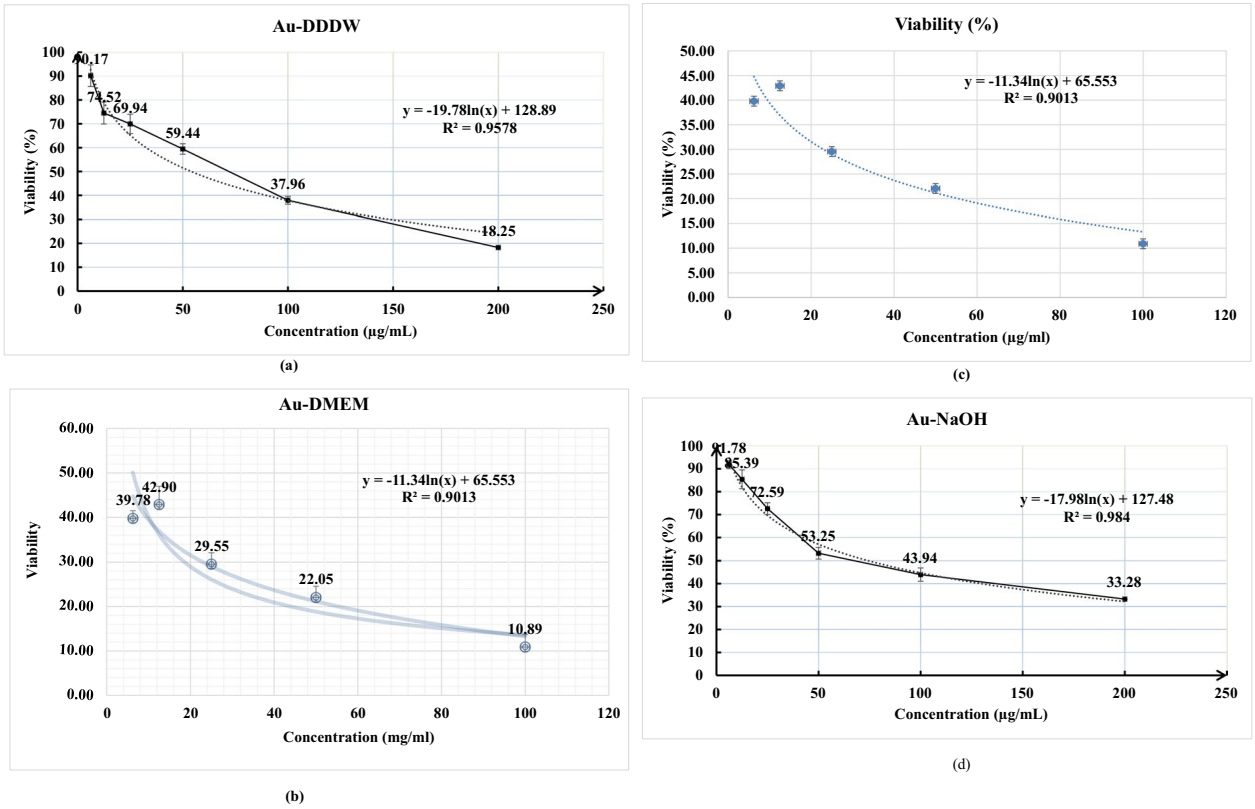

Fig. 8 **a**–**d** Cytotoxicity effects of synthesized AuNPs on Hepa 1–6 mouse cell lines

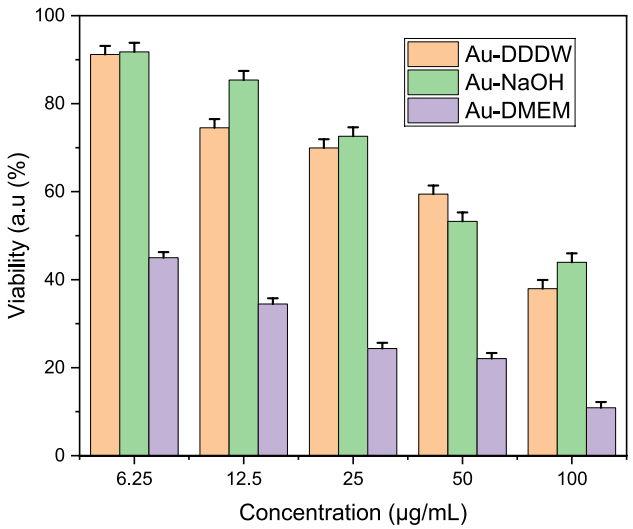

Fig. 9 Holographic representation of the relationship between the concentration of AuNPs and cell survival

This phase was finished during the phases of preparation of the NPs synthesis liquids inside the chemical or biological processes. The AuNPs produced by this method were higher than those produced by DDDW. This resulted in localized displacement of absorption peaks due to AuNPs adsorption of protein molecules inside DMEM. The production of reactive oxygen species (ROS), which results in oxidative stress, is what makes metallic nanomaterials hazardous [30]. By scavenging free radicals, preventing the generation of ROS, and boosting the activity of antioxidant enzymes, AuNPs function as antioxidants [31].

Physical investigations have shown that laser settings and the surrounding media influence the size and concentration of AuNPs. Biological experiments have demonstrated that AuNPs have the ability to bind to cancer cells depending on their size and concentration. The impact of AuNPs grows with the growth of their size in those made with DDDW but begins to diminish with size in those prepared with DMEM. Due to their small size, AuNPs have the ability to infiltrate large areas, deposit themselves on the tumor site, bind to a variety of medicines and biomolecules, target drug delivery, and have good biocompatibility. Positive outcomes in the therapy of cancer may arise from the application of two nanoparticles with distinct uses [32]. Additionally, as an illustration from the comparable relevant prior studies on the sustainable chemistry along with an efficacious drug in the medical-field, the process of biosynthesis, stability, as well as self-assembled characteristics of the Gold Nanoparticles through Chlorella vulgaris extraction [33].

Conclusions

In this study, AuNPs were successfully synthesized using ns-pulsed laser ablation in liquid with three different liquid media, namely DDDW, NaOH, and DMEM. The synthesized NPs were characterized using UV–Vis, XRD, and TEM with atomic force microscopy (AFM) and FTIR. The optical absorption of UV–Vis spectroscopy confirmed the formation of AuNPs, while TEM and AFM analyses demonstrated the presence of crystallinity of the synthesized NPs with the purity of Au compound. XRD analysis verified the particles are of Cub-centered structure and crystalline in nature, and using Debye–Scherrer's formula, the average crystallite size was determined to be 11.4, 19.7, and 8.8 nm from the media, namely DDDW, NaOH, and DMEM.

Analysis was done on the cytotoxicity behavior of the laser ablation AuNPs. According to these findings, cell viability declines as synthesized AuNP concentrations rise. This verified that the test compounds exhibited notable cytotoxic potential properties, with IC50 concentrations of 53.95 µg/ml at the treatment group for gold nanoparticles prepared in double distilled water (DDDW) and 74.38 µg/ml and 35.48 µg/ml at the treatment group for gold nanoparticles prepared in NaOH and culture medium DMEM, respectively.

Therefore, it is advised that AuNPs produced by ns-pulsed laser ablation in liquid with three distinct liquid media have encouraging antibacterial and anticancer effects in vitro and be used for additional nanotherapeutic uses.

However, more research are required in the future to evaluate the in vivo anticancer effects of synthetic AuNPs made utilizing liquid ns-pulsed laser ablation.

Supplementary Information The online version contains supplementary material available at https://doi.org/10.1007/s13404-025-00363-z.

Author contribution Conceptualization, EJK, EYR, ZHJA, KAM, RAMA; formal analysis, EJK, EYR, ZHJA, KAM, RAMA, SS; investigation, EJK, EYR, ZHJA, KAM, RAMA; writing—original draft preparation, EJK, EYR, ZHJA, KAM, RAMA; writing—review and editing, SS, TK, MS, Ankur Kulshreshta (AK), Abhinav Kumar (AK), KR; supervision, TK, MS, Ankur Kulshreshta (AK), Abhinav Kumar (AK), KR; project administration, TK, MS, Ankur Kulshreshta (AK), Abhinav Kumar (AK), KR; funding acquisition, KAM, KR. All authors have read and agreed to the published version of the manuscript.

Data availability The data used to interpret the findings are available from the authors, Entidhar Jasim Khamees, Elaf Yousif Rashid, Zainab Hayder Jabber Al-Kufaishi, and Kahtan A. Mohammed. All the characterizations, analysis, testing's related work and testing's have solely been responsible by Entidhar Jasim Khamees, Elaf Yousif Rashid, Zainab Hayder Jabber Al-Kufaishi, and Kahtan A. Mohammed. Additionally, the raw data can be obtained on request from the corresponding authors, Entidhar Jasim Khamees, Elaf Yousif Rashid, Zainab Hayder Jabber Al-Kufaishi, and Kahtan A. Mohammed.

Declarations

Ethical approval Not applicable.

Consent to participate Not applicable.

Consent for publication All authors have read and approved this manuscript.

Competing interests The authors declare no competing interests.

References

1. Mzwd E, Ahmed NM, Suradi N, Alsaee SK, Altowyan AS, Almessiere MA, Omar AF (2022) Green synthesis of gold nanoparticles in Gum Arabic using pulsed laser ablation for CT imaging. Sci Rep 12(1):10549
2. Al-Tememe EH, Algalal HMAA, Abodood AAF, Mohammed KA, Khamees EJ, Zabibah RS, Abed AS (2022) Anticancer and Antimicrobial activity of PVA/Fe2O3/TiO2 hybrid nanocomposite. Int J Nanosci 21(03):2250018
3. Mohammed KA, Hadi MM, Hussein EH, Al-Kabbi AS, Ziadan KM (2022) Properties and white light photoresponses of CdSe colloidal nanoparticles. In: Materials Science Forum, Trans Tech Publications Ltd, vol 1065, pp 119–126. https://doi.org/10.4028/p-8x77b7
4. Ajam AM, Mohammed KA, Salman ZN (2022) Optical properties of PbS/CdZnS double layers nanocrystalline thin films for optoelectronic applications. Int J Nanosci 21(05):2250037
5. Pang S, Yang T, He L (2016) Review of surface enhanced Raman spectroscopic (SERS) detection of synthetic chemical pesticides. TrAC, Trends Anal Chem 85:73–82
6. Lee SJ, Lee H, Begildayeva T, Yu Y, Theerthagiri J, Kim Y, Choi MY (2022) Nanogap-tailored Au nanoparticles fabricated by pulsed laser ablation for surface-enhanced Raman scattering. Biosensors and Bioelectron 197:113766
7. Sharma B, Frontiera RR, Henry AI, Ringe E, Van Duyne RP (2012) SERS: Materials, applications, and the future. Mater Today 15(1–2):16–25
8. Crisan MC, Teodora M, Lucian M (2021) Copper nanoparticles: Synthesis and characterization, physiology, toxicity and antimicrobial applications. Appl Sci 12(1):141
9. Xu L, Wang YY, Huang J, Chen CY, Wang ZX, Xie H (2020) Silver nanoparticles: Synthesis, medical applications and biosafety. Theranostics 10(20):8996
10. Gamal-Eldeen AM et al (2016) Photothermal therapy mediated by gum Arabic-conjugated gold nanoparticles suppresses liver preneoplastic lesions in mice. J Photochem Photobiol B Biol 163:47–56
11. Fazal-Ur-Rehman M, Qayyum I (2020) Biomedical scope of gold nanoparticles in medical sciences: an advancement in cancer therapy. J Med Chem Sci 3:399–407
12. Zukhi J et al (2017) Evaluation of image quality and radiation dose using gold nanoparticles and other clinical contrast agents in dual energy. IOP Conf Ser J Phys 851:1–8
13. Torrisi L, Torrisi A (2018) Laser ablation parameters influencing gold nanoparticle synthesis in water. Radiat Ef Defects Solids 173:729–739
14. Xi D et al (2012) Gold nanoparticles as computerized tomography (CT) contrast agents. RSC Adv 2:12515–12524
15. De Barros HR et al (2016) Stability of gum arabic-gold nanoparticles in physiological simulated pHs and their selective effect on cell lines. RSC Adv 6:9411–9420

16. Fratoddi I et al (2019) Highly hydrophilic gold nanoparticles as carrier for anticancer copper(I) complexes: loading and release studies for biomedical applications. Nanomaterials 9:772
17. Gao Q, Zhang J, Gao J, Zhang Z, Zhu H, Wang D (2021) Gold nanoparticles in cancer theranostics. Frontiers in bioengineering and biotechnology 9:647905
18. Raheem MA, Rahim MA, Gul I, Zhong X, Xiao C, Zhang H, Qin P (2023) Advances in nanoparticles-based approaches in cancer theranostics. OpenNano 12:100152. https://doi.org/10.1016/j.onano.2023.100152
19. Vinod M, Jayasree RS, Gopchandran KG (2017) Synthesis of pure and biocompatible gold nanoparticles using laser ablation method for SERS and photothermal applications. Curr Appl Phys 17(11):1430–1438
20. Salam JA, Vinod M, Gopchandran KG (2022) Studies on plasmon coupling between pure colloidal gold nanoparticles prepared by laser ablation in water. Materials Today: Proceedings 54:882–889
21. Zhang D, Gokce B, Barcikowski S (2017) Laser synthesis and processing of colloids: fundamentals and applications. Chem Rev 117(5):3990–4103
22. Zhilnikova MI, Barmina EV, Shafeev GA (2020) Laser-assisted generation of elongated Au nanoparticles and analysis of their morphology under pulsed irradiation in water and CaCl2 solutions. In: Journal of Physics: Conference Series, IOP Publishing, VIII International Youth Scientific School-Conference "Modern Problems of Physics and Technology" (MPPT2019) , Moscow, vol 1439, no 1, p 012026. https://doi.org/10.1088/1742-6596/1439/1/012026
23. Khamees EJ, Gençyılmaz O (2024) Comparison of alternative gold nanoparticles (AuNPs) produced by laser ablation technique for photothermal therapy applications. J Opt. https://doi.org/10.1007/s12596-024-01962-3
24. Hammood SA, Abodood AAF, AlGalal HMAA, Khamees EJ, Abbas MF, Zabibah RS, Ameen NI (2022) Synthesis and characterization of PVA–Fe2O3–CuO hybrid structure for biomedical application. Intern J Nanosci 21(04):2250030
25. Al-Tememe EH, Al Hasan NHJ, Kareem AS, Salem KH, Khmees EJ, Zabibah RS, Mohammed KA (2023) Designing PMMA-PVA-TiO2 as new hybrid nanocomposite for anticancer applications. Int J Nanosci 22(04):2350029. https://doi.org/10.1142/S0219581X23500291
26. Jarad AN, Talib RA, Kareem AS, Mohammed JH, Khmees EJ, Salem KH, Saxena KK (2023) Studying the optical and structural properties and anticancer activity of new PVA–Fe2O3: Cu nanocomposite materials. Intern J Nanosci 22(02):2350015
27. Zhang C, Zhang W, Karadas F, Low J, Long R, Liang C, Xiong Y (2022) Laser-ablation assisted strain engineering of gold nanoparticles for selective electrochemical CO 2 reduction. Nanoscale 14(20):7702–7710
28. Bennett WE, Broberg DE, Baenziger NC (1973) Crystal structure of stannic phthalocyanine, an eight-coordinated tin complex. Inorg Chem 12(4):930–936
29. Stetsenko MO, Rudenko SP, Maksimenko LS, Serdega BK, Pluchery O, Snegir SV (2017) Optical properties of gold nanoparticle assemblies on a glass surface. Nanoscale Res Lett 12(1):348
30. Vahideh H, Alireza H, Reza M, Rezai GA, Yazdi MET (2024) Fabrication and characterization of gold nanoparticles using alginate: *in vitro* and *in vivo* assessment of its administration effects with swimming exercise on diabetic rats. Open Life Sci 19(1):20220869. https://doi.org/10.1515/biol-2022-0869
31. Shakerimanesh K, Bayat F, Shahrokhi A, Baradaran A, Yousefi E, Mashreghi M, Yazdi MET (2022) Biomimetic synthesis and characterisation of homogenouse gold nanoparticles and estimation of its cytotoxity against breast cancer cell line. Mater Technol 37(13):2853–2860. https://doi.org/10.1080/10667857.2022.2081287
32. Mousavi-Kouhi SM, Beyk-Khormizi A, Amiri MS, Mashreghi M, Hashemzadeh A, Mohammadzadeh V, Alavi F, Mottaghipisheh J, Sarafraz Ardakani MR, Taghavizadeh Yazdi ME (2023) Plant gel-mediated synthesis of gold-coated nanoceria using Ferula gummosa: characterization and estimation of its cellular toxicity toward breast cancer cell lines. Journal of Functional Biomaterials 14(7):332. https://doi.org/10.3390/jfb14070332
33. Annamalai J, Nallamuthu T (2015) Characterization of biosynthesized gold nanoparticles from aqueous extract of chlorella vulgaris and their anti-pathogenic properties. Appl Nanosci 5(5):603–607